



Kinetics of CO₂ methanation on a Ru-based catalyst at process conditions relevant for Power-to-Gas applications

Leonardo Falbo^a, Michela Martinelli^a, Carlo Giorgio Visconti^{a,*}, Luca Lietti^a, Claudia Bassano^b, Paolo Deiana^b

^a Politecnico Di Milano, Dipartimento di Energia, Milano, 20156, Italy

^b ENEA, Santa Maria di Galeria, Roma, 00123, Italy



ARTICLE INFO

Keywords:

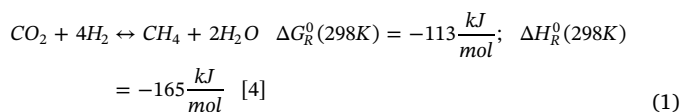
CO₂ methanation
Sabatier reaction
Power-to-gas
Ru/γ-Al₂O₃ catalyst
Kinetics
Water effect

ABSTRACT

In this paper we show that a 0.5 wt.% Ru/γ-Al₂O₃ catalyst is appropriate to carry out the Sabatier reaction (CO₂ methanation) under process conditions relevant for the *Power-to-Gas* application and we provide a kinetic model able to describe the CO₂ conversion over a wide range of process conditions, previously unexplored. To achieve these goals, the effects of feed gas composition (H₂/CO₂ ratio and presence of diluents), space velocity, temperature and pressure on catalyst activity and selectivity are investigated. The catalyst is found stable when operating over a wide range of CO₂ conversion values, with CH₄ selectivity always over 99% and no deactivation, even when working with carbon-rich gas streams. The effect of water on the catalyst performance is also investigated and an inhibiting kinetic effect is pointed out. Eventually, the capacity of kinetic models taken from the literature to account for CO₂ conversion under the explored experimental conditions is assessed. It is found that the kinetic model proposed by Lunde and Kester in 1973 (*J. Catal.* 30 (1973) 423) is able to describe satisfactorily the catalyst behavior in a wide range of CO₂ conversion spanning from differential conditions to thermodynamic equilibrium, provided that a new set of kinetic parameters is used. It is shown however that a better fitting can be achieved by using a modified kinetic model, accounting for the inhibiting effect of H₂O on CO₂ conversion rate.

1. Introduction

The abatement of CO₂ emissions and the use of renewable sources to produce electricity play key roles towards carbon neutral energy balance [1,2]. An option to combine these two strategies is the chemical reduction of CO₂ to CH₄ using renewable hydrogen [3]. According to this process, which is referred to as *Power-to-Gas* (*PtG*) process, renewable or excess electric energy is used for H₂O electrolysis and produced H₂ is then combined with (captured) CO₂ and converted to CH₄ (synthetic or substitute natural gas, SNG) through the Sabatier reaction (Eq. (1)).



With respect to other fuels, SNG has the advantage that can be directly injected into existing natural gas pipeline network and used – when and where needed – as such or for the production of electricity or

chemicals [5]. This technology is used at industrial scale by Audi at Wertle (Germany): this facility produces around 1000 tpa of SNG from concentrated CO₂ obtained from biogas, allowing to recycle about 2800 tpa of CO₂ [6–8]. Nowadays, several other pilot plants are under construction [3,9].

Even if the Sabatier reaction (Eq. (1)) is thermodynamically favorable, the reduction of fully oxidized carbon to methane occurs through an eight-electrons process with significant kinetic limitations [10]. A suitable catalyst is thus required to achieve acceptable process performance [11]. Metals, such as ruthenium, rhodium, nickel and cobalt on various supports are effective catalysts [12–14]. Over the last years, Ni-based catalysts have been widely investigated because of their low cost and wide availability [11]. The literature reports that high activation temperatures are needed to achieve the maximum CO₂ conversion, which results in undesirable influences on the catalyst stability/lifetime as well as in increased energy consumption [15]. Also, it has been shown that the interaction between the Ni particles and adsorbed CO forms mobile/volatile nickel carbonyls, which lead to the loss/sintering of the metal particles [16–18]. Eventually, undesired co-production of

* Corresponding author.

E-mail address: carlo.visconti@polimi.it (C.G. Visconti).

CO through the reverse-water-gas-shift reaction can be relevant on Ni catalysts depending on metal loading, preparation method and pre-treatment conditions [4,19,20].

Noble metals are reported to be more active than nickel in the CO₂ hydrogenation [11,12,21]. For example, 96% yield to methane with no CO co-production can be obtained at 300 °C on 3% Ru/γ-Al₂O₃, while the maximum CH₄ yield for 20% Ni/γ-Al₂O₃ is 80% at 400 °C with some CO co-production [21]. Furthermore, noble metals are reported to be more tolerant than nickel to deterioration due to lower sulphur poisoning, carbon deposition or carbides formation [12,22]. In particular, ruthenium supported on metal oxide carriers like Al₂O₃, TiO₂, CeO₂ or SiO₂ exhibits higher activity than the other noble metals [12,14,23–26]. Solymosi and Erdöhelyi [23], working with 5 wt.% noble metal alumina-supported catalysts prepared using metal chlorides, have proved that the specific CO₂ methanation rate decreases in the order Ru > Rh > Pt ~ Ir ~ Pd, with turnover numbers for Ru and Rh two orders of magnitude higher than the other metals. Similar ranking of noble metals has been also reported by De Leitenburg et al. [24] using CeO₂ as support. Regarding the process selectivity, Ru- and Rh-based catalysts are more selective to methane than Pt- and Pd-based ones, which lead to high CO selectivity [25]. Accordingly, Ru-based catalysts are the optimal candidates for CO₂ methanation with the scope of process intensification. This seems indeed an economically sustainable option considering that the required metal loading is rather low [27].

The reaction pathway of CO₂ methanation is still under debate and there is evidence that the nature of the metal, the typology of the support and process conditions can affect the reaction mechanism. Focusing on Ru-based alumina-supported catalysts, FTIR spectroscopy showed that adsorbed CO on ruthenium sites is a key reaction intermediate [28–32]. The CO₂ activation pathway is however still under debate: some authors propose CO₂ is dissociatively adsorbed on the catalyst surface to form CO and O ad-species [31,33], which are then hydrogenated, while other studies suggest the H-assisted CO₂ dissociation through the formation of bicarbonate and formate species on the support [34–36]. Eventually, the pathways involved in the subsequent CO dissociation mechanism are also not clear and both H-assisted [35] and unassisted [37] routes are suggested.

For what concerns the process kinetics, Table 1 shows the empiric CO₂ conversion rate equations available in the open literature [21,22,34–44]. Notably, most of these models have been developed using experimental data collected at atmospheric pressure. Furthermore, in most of the cases data have been collected at low CO₂ conversion values (< 10%) to ensure differential conditions, or working with very diluted inlet stream. Power law equations, which do not account for the approach to equilibrium, show that at low CO₂ conversion values the reaction rate has a dependence on H₂ partial pressure (reported reaction order in the range 0.3–2.5) stronger than on CO₂ (reaction order 0–1).

No valuable information can be derived from most of these models at the conditions of industrial interest for PtG applications. One exception is the case of the empirical model proposed in 1973 by Lunde and Kester [22] (Eq. (2)), which is potentially able to predict the catalyst activity from differential to thermodynamically limited CO₂ conversions.

$$r_{CO_2} = k \left\{ [P_{CO_2}]^n [P_{H_2}]^{4n} - \frac{[P_{CH_4}]^n [P_{H_2O}]^{2n}}{(K_{eq}(T))^n} \right\} \quad (2)$$

Even if the model proposed by [22] has been fitted by the authors to data collected under differential conditions, the same rate equation has been indeed successively used by other authors [42,43] to fit experimental data collected in a larger range of CO₂ conversion. It has been shown, however, that the value of the parameter *n* drastically changes to describe the catalyst performance at high CO₂ conversion.

A dedicated comment must be made on the ability of the models based on Eq. (2) to describe data collected under pressure. The original

model proposed by Lunde and Kester [22] has been developed using data collected at atmospheric pressure. Recently it has been successfully validated [45] using experimental data collected under pressure [46]. Unfortunately, however, data used for model validation approach the thermodynamic equilibrium.

On these bases, studies considering the behavior of commercial catalytic materials under experimental condition typical of the *Power-to-Gas* technology are still lacking, and this has motivated our study. Accordingly, the goal of this work is to provide a quantitative description of the performance of a representative Ru-based catalyst with a low metal loading, under process conditions of interest for intensified *Power-to-Gas* processes. To the scope, the performance of a 0.5 wt.% Ru/Al₂O₃ commercial material in the CO₂ methanation has been extensively investigated, analyzing the effect of the process conditions (T, P, GHSV, feed composition) on catalyst stability, activity and selectivity in a wide range of CO₂ conversion. The influence of water on the catalyst performance and in the process kinetics has been also investigated. Eventually, Eq. (2) has been fitted to our data and a novel modified kinetic expression has eventually been proposed granting a very good fit of experimental data.

2. Experimental

2.1. Catalytic material and characterization

The reference catalyst adopted in this work is a 0.5 wt.% Ru/Al₂O₃ commercial material (Aldrich, 206199, CAS = 1344–28–1, MDL = MFCD00011207). The purchased catalytic material has a cylindrical shape with a characteristic length (defined as volume to surface ratio) of 3.2 mm. Cutting a single pellet orthogonally to its symmetry axis and analyzing it by optical microscopy, the material shows an eggshell active phase distribution, with a shell thickness of 210 ± 20 μm (Fig. 1(a)).

Micrographs of the sample were obtained by using an optical microscope (Olympus SZ40) connected to a camera (Infinity 2) equipped with an image analysis software (Image-Pro plus) and by using a scanning electron microscope (Zeiss EVO50 EP) equipped with an energy dispersive X-ray spectrometer (Oxford Inca Energy 200 – Pentafet LZ4). The amount of ruthenium in the shell, estimated with SEM-EDX, is around 4.5 wt.% and it decreases moving towards the pellet axis (Fig. 1(b)).

For the activity study, the catalyst pellets were crushed and sieved below 106 μm to avoid the reagent by-passes of the catalyst bed and to limit intra-porous mass transfer limitation.

Textural properties of the powdered sample were determined, using the BET method, by N₂ adsorption-desorption isotherms, measured at –196 °C with a Micromeritics Tristar 3000 instrument. Prior to the analysis, the sample was evacuated at 120 °C for 3 h. Powder X-ray Diffraction (XRD) analyses were performed by a Bruker D8 instrument exploiting a Cu-Kα radiation in a 2θ range of 20–70°, using a counting time of 12.5 s per step.

Once powdered, the catalyst has a BET area of 103 m²/g and a pore volume of 0.24 cm³/g, corresponding to an average pore diameter of 94 nm. XRD analysis (Fig. 2) shows the presence of crystalline γ-Al₂O₃ and microcrystalline RuO₂.

2.2. Catalyst testing

Activity tests were carried out in a lab-scale rig operating 24/7. The unit was equipped with a fixed-bed reactor (I.D. 1.1 cm, length 23 cm), placed into a tubular electric furnace. Experimental data at atmospheric pressure were collected using a quartz reactor, while data at higher pressures were collected with a stainless steel (316L) reactor.

Mass flow controllers (Brooks Instrument, 5820S) were used to regulate the flow rates of the reactants. Bourdon manometers and a piezoresistive pressure transducer (Swagelok, PTI-S-NG100-12AQ)

Table 1
Overview of kinetic models on Ru-based catalysts reported in literature.

Equation rate	E_A [kJ/mol]	Reaction orders	Catalyst	T [°C]	P [ata]	H_2/CO_2 [mol/mol]	GHSV [L/h]	$P_{H_2O}^0$ [ata]	χ_{CO_2} [%]	Ref.
$r = k(P_{H_2})^n H_2$	60	$n_{H_2} = 0.39$	3%Ru/ γ -Al ₂ O ₃	220–300	1	3–15	5500	0.6–0.9	0	3–7 [21]
$r = k(P_{CO_2})^n CO_2 (P_{H_2})^n H_2$	57–70	$n_{CO_2} = 0.1$	0.5%Ru/ γ -Al ₂ O ₃	240–300	1	0.7–7	33000–135000	0.2–0.8	–	< 5 [35]
	64–80	$n_{H_2} = 0.3 – 0.5$	5%Ru/ γ -Al ₂ O ₃							
$r = k(P_{CO_2})^n CO_2 (P_{H_2})^n H_2$	60 ± 12	$n_{CO_2} = 0.14 – 0.28$	0.5%Ru/ γ -Al ₂ O ₃ 0.8%Ru/ γ -Al ₂ O ₃	300–380	1	4.2	–	0–0.5	–	0–5 [38]
		$n_{H_2} = 0.46 – 0.87$								
$r = k(P_{CO_2})^n CO_2 (P_{H_2})^n H_2$	64	$n_{CO_2} = 0.47$	5%Ru/ γ -Al ₂ O ₃	170–230	1	–	3000–6000	–	–	6–10 [36]
		$n_{H_2} = 1$								
$r = k(P_{CO_2})^n CO_2 (P_{H_2})^n H_2 (P_{H_2O})^n H_2 O$	80 ± 4	$n_{CO_2} = 0.22$	2%Ru/TiO ₂	363–413	–	–	0.5–0.85 [mol/mol]	0.0008–0.0121	–	[30]
		$n_{H_2} = 0.57$								
$r = k(P_{CO_2})^n CO_2 (P_{H_2})^n H_2 (P_{H_2O})^n H_2 O$	81	$n_{CO_2} = 1$	Ru Raney Ru/SiO ₂	70–110	0.8	2	–	–	–	0–30 [39]
		$n_{H_2} = 2.5$								
$r = k(P_{CO_2})^n CO_2 (P_{H_2})^n H_2 (P_{H_2O})^n H_2 O (P_{CH_4})^n CH_4$	66	$n_{CO_2} = 0.34$	10%Ru/ γ -Al ₂ O ₃	200–245	1	4–6	90000–262920	0.3–0.9	0.03–0.1	< 10 [40]
		$n_{H_2} = 0.88$								
		$n_{H_2O} = -0.23$								
$r = k(P_{CO_2})^n CO_2 (P_{H_2})^n H_2 (P_{H_2O})^n H_2 O (P_{CH_4})^n CH_4$	n.a.	$n_{CH_4} = -0.11$	3.8%Ru/TiO ₂	150–210	1	4	–	> 0.7	0–0.15	< 10 [37]
		$n_{H_2} = 0.5$								
		$n_{H_2O} = -0.2 \div -0.5$								
		$n_{CH_4} = \sim 0$								
$r = k \left\{ [P_{CO_2}]^n [P_{H_2}]^{4n} - \frac{[P_{CH_4}]^n [P_{H_2O}]^{2n}}{(K_c(T))^n} \right\}$	71	$n = 0.225$	0.5%Ru/Al ₂ O ₃	200–350	1	2–4	3000–7700	0	0–0.5	0–18 [22,41]
$r = k \left\{ [P_{CO_2}]^n [P_{H_2}]^{4n} - \frac{[P_{CH_4}]^n [P_{H_2O}]^{2n}}{(K_c(T))^n} \right\}$	69	$n = 0.85$	0.5%Ru/Al ₂ O ₃	200–445	2	1–5	100–450	–	–	20–100 ^a [42]
$r = k \left\{ [P_{CO_2}]^n [P_{H_2}]^{4n} - \frac{[P_{CH_4}]^n [P_{H_2O}]^{2n}}{(K_c(T))^n} \right\}$	69	$n = 0.3$	3%Ru/TiO ₂	300–450	1	3.6	45000	0.05	0	50–70 ^a [43]

^a Thermodynamic equilibrium for high value of CO₂ conversion.

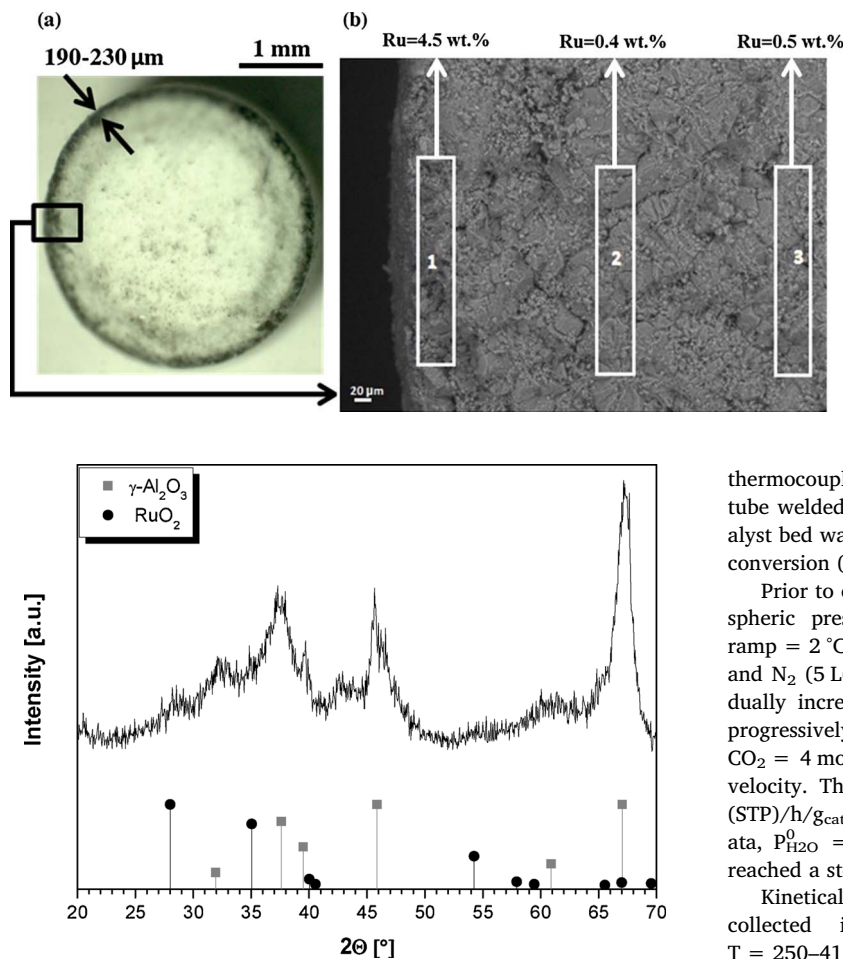


Fig. 1. (a) Optical micrograph of a Ru/Al₂O₃ pellet cut orthogonally to the axis.
(b) SEM micrograph and results of EDX analysis.

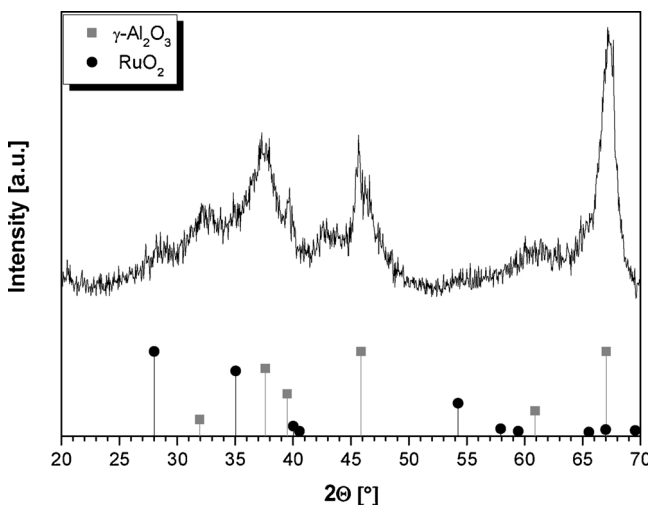


Fig. 2. XRD patterns of powdered catalyst.

were used to check the working pressure of the catalyst bed. A high precision syringe pump (ISCO, 100 DX), connected directly to the catalytic bed by a silica capillary tube, was used for water co-feeding experiments. The unconverted gases and the reaction products leaving the reactor were sent to a cold trap, kept at 0 °C by using a circulation chiller (Lauda, MC 350), in order to condense the water produced. The accumulated water was removed from the trap every 12 h. The transfer line connecting the reactor with the trap was kept at 150 °C to prevent the condensation of water.

Reactants and products were analyzed by using an on-line gas chromatograph (Agilent, 6890) equipped with two wide-bore columns each connected to a thermal conductivity detector (TCD). A molsieve 5 Å particle trap column (Agilent, 7538, 25 m × 0.53 mm × 50 μm) connected to the first TCD was used to quantify H₂, Ar, N₂, CH₄ and CO concentrations, while a PoraPlot Q particle trap column (Agilent, 7554, 25 m × 0.53 mm × 20 μm) connected to the second TCD was used to detect CO₂ and light hydrocarbons. No traces of C₂₊ hydrocarbons were detected in the products. The carbon balance, calculated using Ar as internal standard, defined as ratio among the total amounts of carbon in the products and the converted CO₂, always closed at 100 ± 3%.

In a typical run, 0.375 g of powdered catalyst (< 106 μm) were diluted with α-Al₂O₃ and loaded in the reactor. A 1 to 1 volumetric dilution was selected to distribute the heat produced by the reaction along the reactor axis and to prevent hot-spot phenomena. In order to keep isothermal conditions along the catalyst bed, the reactor was also shielded with an aluminum foil and the temperature of the reactor was controlled using a PID controller (Eurotherm, 3216) exploiting the reading of a J-type thermocouple placed at the inlet of the catalyst bed. The axial temperature profile was monitored with a second J-type

thermocouple sliding in an axial thermowell (2 mm O.D. stainless steel tube welded on one side). The differential temperature along the catalyst bed was always lower than 3 °C, even when working at high CO₂ conversion (i.e., high reaction heat produced).

Prior to each run, the catalyst was activated by reduction at atmospheric pressure using H₂ (1.8 L(STP)/h/g_{cat}) at 400 °C (heating ramp = 2 °C/min) for 3 h. Then the reactor was cooled down to 250 °C and N₂ (5 L(STP)/h/g_{cat}) was fed. The catalyst temperature was gradually increased to 350 °C (heating ramp = 1 °C/min), N₂ flow was progressively decreased and, simultaneously, reactants stream (H₂/CO₂ = 4 mol_{H2}/mol_{CO2}) was fed, keeping constant the total gas space velocity. The achieved process conditions (T = 350 °C, GHSV = 5 L(STP)/h/g_{cat}, P = 1 ata, H₂/CO₂ = 4 mol_{H2}/mol_{CO2}, P_{N2}⁰ + Ar = 0.1 ata, P_{H2O}⁰ = 0 ata) were kept unchanged until CO₂ conversion rate reached a steady value.

Kinetically relevant CO₂ conversion and CH₄ selectivity data were collected in the following ranges of process conditions: T = 250–410 °C, P = 1–7 ata, GHSV = 3.75–10.00 L(STP)/h/g_{cat}, H₂/CO₂ inlet ratio = 1–5 mol_{H2}/mol_{CO2} (using N₂ as diluent so to vary P_{H2}⁰ while keeping P_{CO2}⁰ constant at 0.15 ata or to vary P_{CO2}⁰ while keeping P_{H2}⁰ constant at 0.46 ata), P_{N2}⁰ + Ar = 0.01–0.4 ata and P_{H2O}⁰ = 0–0.29 ata. Each effect was studied keeping constant the other process conditions at the central values (T = 310 °C, P = 1 ata, GHSV = 5 L(STP)/h/g_{cat}, H₂/CO₂ = 4 mol_{H2}/mol_{CO2}, P_{N2}⁰ + Ar = 0.1 ata, P_{H2O}⁰ = 0 ata) and varying the desired one. Table 2 reports the investigated process conditions, each of which was replicated several times in order to verify data accuracy and reproducibility. Moreover, a reference condition, corresponding to the central point in Table 2, was replicated with a frequency higher than every 24 h in order to evaluate the catalyst stability. Notably, the experimental data used in this work were collected in three different runs carried out adopting each time fresh catalyst from the same batch. The reproducibility of the results obtained in the three runs was also verified by comparing the catalyst activity and selectivity at the reference conditions (central point, Table 2).

H₂O co-feeding experiments were performed using ultra-pure water (Carlo Erba Reagents, 412180) so to avoid any possible effect related to the presence of impurities in the co-fed stream. Water concentration was varied in the 0–29 mol% range and, upon water addition, nitrogen flow rate was decreased in order to keep the GHSV constant. The relative amount of water fed ($F_{H_2O}^{IN}$) with respect to that produced by the reaction during the dry run at the same T, P, GHSV and H₂/CO₂ ratio ($F_{H_2O,R}$) was described by the following parameter (β) (Eq. (3)).

$$\beta = \frac{F_{H_2O}^{IN}}{F_{H_2O,R}} \quad (3)$$

2.3. Assessment of transfer limitation

In order to verify the absence of external mass transfer limitation,

Table 2
Experimental plan.

	T [°C]	P [ata]	GHSV [L(STP)/h/g _{cat}]	H ₂ /CO ₂ [mol/mol]	Molar composition [-]				Included in dataset:
					H ₂	CO ₂	N ₂ + Ar	H ₂ O	
Central point	310	1	5.00	4.00	0.72	0.18	0.10	0	1; 2
T-effect	250–410	1	5.00	4.00	0.72	0.18	0.10	0	1; 2
P-effect	290;310	1–7	5.00	3.90	0.78	0.20	0.02	0	2
GHSV-effect	290;310	1	3.75–10.00	4.00	0.72	0.18	0.10	0	1; 2
H ₂ /CO ₂ -effect (P _{H2} ⁰ = cost)	310	1	5.00	1.03–5.00	0.46	0.44–0.09	0.10–0.45	0	1; 2
H ₂ /CO ₂ -effect (P _{CO2} ⁰ = cost)	310	1	5.00	2.00–5.00	0.30–0.75	0.15	0.55–0.10	0	1; 2
Dilution-effect	310	1	5.00	4.00	0.72–0.48	0.18–0.12	0.10–0.40	0	1; 2
H ₂ O-effect	310	1	5.00	4.00	0.56	0.14	0.30–0.01	0–0.29	1; 2

two activity tests were carried out using different amounts of catalyst loading in the reactor (0.375 g and 0.75 g, respectively) and the same GHSV values. In both the tests, the catalyst was activated with the procedure reported in Section 2.2 and, after the initial transient, the process conditions were set at T = 310 °C, P = 1 atm, H₂/CO₂ = 4 mol_{H2}/mol_{CO2}, P_{N2 + Ar}⁰ = 0.1 atm. During both the tests, the space velocity was varied in the range 3.75–7.50 L(STP)/h/g_{cat}.

At the same space velocity (GHSV), the two catalytic beds worked with different linear velocity. Nevertheless, Fig. 3 shows that in both the tests the same CO₂ conversion was measured at given space velocity, clearly indicating the absence of external mass transfer limitations.

The absence of mass and heat, intra and inter-phase limitations was also theoretically checked by using the empirical criteria proposed by Mears [47] (Table 3). The fluid dynamic proprieties were estimated using the databases included in the software Aspen HYSYS®. Heat and mass transfer coefficients were estimated by correlation equations reported by Wakao et Kaguei [48]. Criteria were checked in the most demanding conditions and they were safely verified.

2.4. Kinetic modeling

For all the kinetic equations evaluated in this work, the rate constant was treated as Arrhenius-type (Eq. (4)).

$$k = k_0 \cdot \exp\left(-\frac{E_A}{R \cdot T}\right) \quad (4)$$

When estimating the values of k₀ and E_A, Eq. (4) was parameterized as shown in Eq. (5) (T_{ref} = 310 °C) so to minimize the correlation index between the pre-exponential factor and the activation energy.

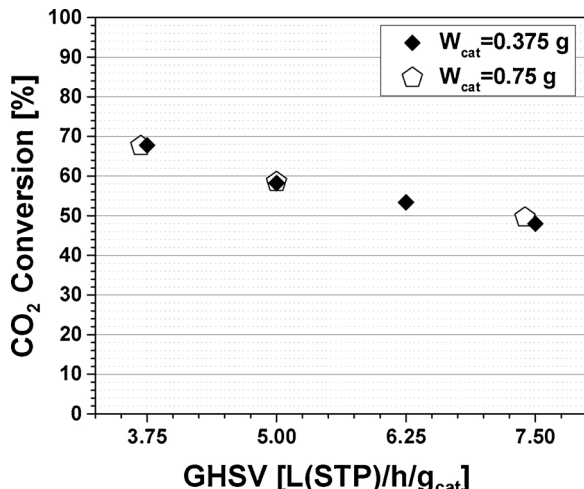


Fig. 3. Experimental check of the absence of external mass transfer limitations.
(Process conditions: T = 310 °C, P = 1 atm, H₂/CO₂ = 4 mol_{H2}/mol_{CO2}, P_{N2 + Ar}⁰ = 0.1 atm).

Table 3
Empirical criteria for ruling at the presence of transport limitation.

	Mass transfer	Heat transfer
Inter-phase	$\frac{r_{eff} \rho_{cat} d_{cat}}{h m' C O_2} < 0.3$	$\frac{r_{eff} \Delta H \rho_{cat} d_{cat}}{h_i T} < \frac{0.3 RT}{E_A}$
Intra-phase	$\frac{r_{eff} \rho_{cat} d_{cat}^2}{4 D_{CO_2}^{eff} C CO_2} < 1$	$\frac{r_{eff} \rho_{cat} d_{cat}^2}{4 D_{CO_2}^{eff} T} < \frac{0.75 RT}{E_A}$

$$k = k_0^* \cdot \exp\left(-\frac{E_A}{R}\left(\frac{1}{T} - \frac{1}{T_{ref}}\right)\right) \quad (5)$$

The value of K_{eq}(T) equilibrium constant was evaluated using the empirical correlation (Eq. (6)) reported by [22].

$$K_{eq}(T) = \exp\left[\left(\frac{1}{1.987}\right) \cdot \left(\frac{56000}{T^2} + \frac{34633}{T} - 16.4 \cdot \ln T + 0.00557 \cdot T\right) + 33.165\right] \quad (6)$$

Developed kinetic expressions were integrated using an isothermal homogeneous plug-flow reactor model. The reactor model is composed by 5 ordinary differential equations (Eq. (7)), expressing the material balances of the main species involved in the process (CO₂, H₂, CH₄, H₂O, N₂), with the initial conditions (Eq. (8)).

$$\frac{dF_i}{dW_{cat}} = \nu_i \cdot r_{Sabatier} \quad (7)$$

$$F_i = F_i^{IN} |_{W_{cat}=0} \quad (8)$$

In Eqs. (7)–(8) F_i and F_i^{IN} are the molar flows of the generic species ith along the reaction axis and at the reactor inlet, respectively, W_{cat} is the catalyst weight, ν_i is the stoichiometric coefficient for ith component and r_{Sabatier} is the Sabatier reaction rate. The presence of CO in the products, whose selectivity was below 1% in most of the investigated process conditions, was neglected in our model.

Kinetic parameters were estimated by performing a nonlinear regression based on the least-square method, using the Fortran subroutine BURENL [49]. The mass balances were integrated numerically with the Fortran subroutine LSODI [50] that allows to solve stiff problems using implicit integration methods with variable step. Based on the extra-diagonal terms of the correlation matrix, each calculated kinetic parameter was not statistically correlated with the others.

The two rate expressions considered in this work are reported in Table 4. The first one is the expression with three kinetic parameters proposed by Lunde and Kester [22]. In this equation, the ratio of the reaction orders for H₂ and CO₂ is fixed at 4. Because the kinetic parameters reported in [22] had been obtained considering only CO₂ conversion data at atmospheric pressure, with the aim of obtaining parameters directly comparable to those given in [22], we decided, as first attempt, to estimate the value of these parameters using a reduced input dataset where the effect of P was not considered (Dataset 1 in

Table 4

Adopted rate expressions and estimated kinetic parameters. The mean percentage error (MPE) is also given.

Tag	Dataset	Equation	k_0 [mol/(sg _{cat} ata ⁵ⁿ)]	E_A [kJ/mol]	n [-]	α [1/ata]	MPE [%]
Lunde [Dataset 1]	1	$r_{CO_2} = k \left\{ [P_{CO_2}]^n [P_{H_2}]^{4n} - \frac{[P_{CH_4}]^n [P_{H_2O}]^{2n}}{(K_{eq}(T))^n} \right\}$	18.26 ± 0.06	68.1 ± 0.3	0.140 ± 0.001	–	5.11
Lunde [Dataset 2]	2		9.37 ± 0.01	65.2 ± 0.2	0.076 ± 0.001	–	4.91
LundeWI [Dataset 2]	2	$r_{CO_2} = \frac{k}{1 + \alpha P_{H_2O}} \left\{ [P_{CO_2}]^n [P_{H_2}]^{4n} - \frac{[P_{CH_4}]^n [P_{H_2O}]^{2n}}{(K_{eq}(T))^n} \right\}$	95.43 ± 0.4	75.3 ± 0.3	0.152 ± 0.001	0.91 ± 0.01	2.76

Table 2). The resulting model is indicated by the “Lunde [Dataset 1]” tag in **Table 4**. As second step, all the experimental data collected in this work, including those collected at pressures higher than atmospheric (Dataset 2 in **Table 2**) were used in the regression, obtaining the “Lunde [Dataset 2]” model.

The second rate expression used in this work was developed by modifying the reaction rate proposed in [22] introducing an additional parameter (α), which changes the kinetic dependence on H₂O partial pressure. This rate expression was fitted to the complete dataset (Dataset 2 in **Table 2**), obtaining the model reported as “LundeWI [Dataset 2]” in **Table 4**.

3. Results and discussion

3.1. Reactivity study

3.1.1. Start-up

CO₂ conversion and CH₄ selectivity trends in the first 40 h on stream, shown in **Fig. 4**, point out that the catalyst progressively gains activity, always keeping a methane selectivity over 99%, the rest being CO.

Notably, the increase of the reaction rate with T.O.S. has been already reported in literature for Ru/Al₂O₃ catalysts. It has been explained either as slow completion of the catalyst reduction process [21], or as loss of the residual chlorine remaining in the catalyst after its preparation using RuCl₃·xH₂O as precursor [51]. Unfortunately, we do not have information on the catalyst precursors and preparation method: this prevents us to definitely assess the reason behind the initial catalyst behavior.

After 40 h on stream, the catalyst reaches steady state conditions in

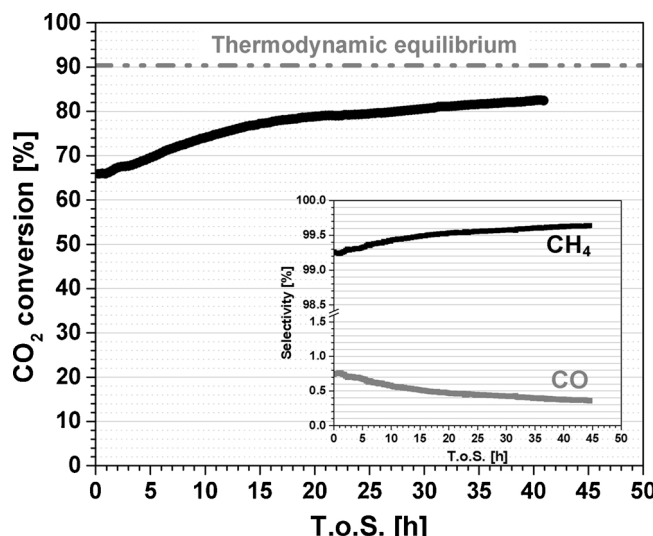


Fig. 4. CO₂ conversion during the start-up. (Inset) CO and CH₄ selectivity during the start-up.

(Process conditions: T = 350 °C, P = 1 ata, GHSV = 5 L(STP)/h/g_{cat}, H₂/CO₂ = 4 mol_{H2}/mol_{CO2}, P_{N2}⁰ + Ar = 0.1 ata).

terms of both activity and selectivity. Accordingly, we started collecting kinetically relevant data. During the study, the catalyst performance was always stable and no deactivation phenomena occurred even after testing at critical conditions as high temperature or by increasing the amount of water in the inlet feed. The possibility to achieve high CO₂ conversion with CH₄ selectivity over 99% confirm the potential of Ru-based catalysts to be used for “once-through” operations in the Sabatier process.

3.1.2. Effects of the process conditions

3.1.2.1. Effect of temperature.. The effect of temperature in the range 250–410 °C is shown in **Fig. 5(a)**, where CO₂ conversion at the thermodynamic equilibrium is also plotted. CO₂ conversion is 14% at 250 °C and increases until a maximum of 87% at 370 °C. By further increasing the temperature, CO₂ conversion decreases due to the approach to thermodynamic equilibrium.

In the investigated T-range, methane is by far the main carbon containing product (selectivity higher than 99.5%, inset of **Fig. 5(a)**), the rest being CO. Notably, these results confirm the almost complete selectivity to methane reported in literature for Ru-based catalysts [25,36], especially at Ru-loading high enough to form Ru clusters [52].

3.1.2.2. Effect of pressure.. Pressure plays an important role in designing a process for the production of SNG. Considering the P-effect on thermodynamics, it is reported that the performance of PtG technology may be optimized if the CO₂ methanation reactor is operated with a pressure in the 5–20 ata range [3,8,9]. Under these conditions, indeed, the thermodynamic constraints are less strict and equipment volumes are decreased. Nevertheless, in literature, there is only one experimental study on Ru-based catalysts for CO₂ methanation accounting for the effect of pressure [46]. In such a work the pressure effect was studied using a Ru/ZrO₂ catalyst, operating at H₂/CO₂ = 4 mol_{H2}/mol_{CO2}, y_{N2}⁰ = 0.5, T = 350 °C and pressure in the 1–20 ata range. It is shown that the activity increases upon increasing the pressure. Unfortunately, however, due to the high temperature adopted, data reported in [46] at pressure over 5 ata are controlled by thermodynamics.

In order to evaluate the effect of pressure on the process kinetics, our catalyst was tested in the range 1–7 ata both at 310 °C and at 290 °C. **Fig. 5(b)** shows the effect of pressure on catalyst activity and selectivity (inset).

CO₂ conversion is kinetically boosted by raising the pressure. At 310 °C it increases from a 58% at atmospheric pressure to 80% at 4 ata and to 87% at 7 ata. The P-effect observed at 290 °C, temperature at which the catalyst works at conditions far from thermodynamic equilibrium, is ever stronger.

In addition to CO₂ conversion, pressure boosts CH₄ selectivity, which reaches 99.9% at 7 ata. Notably, even if ruthenium is usually reported to be very active in the Fischer-Tropsch synthesis at high pressure [53], no evidence of C₂₊ hydrocarbons or oxygenates species have been detected in the products under the adopted process conditions.

3.1.2.3. Effect of space-velocity.. The effect of GHSV on CO₂ conversion

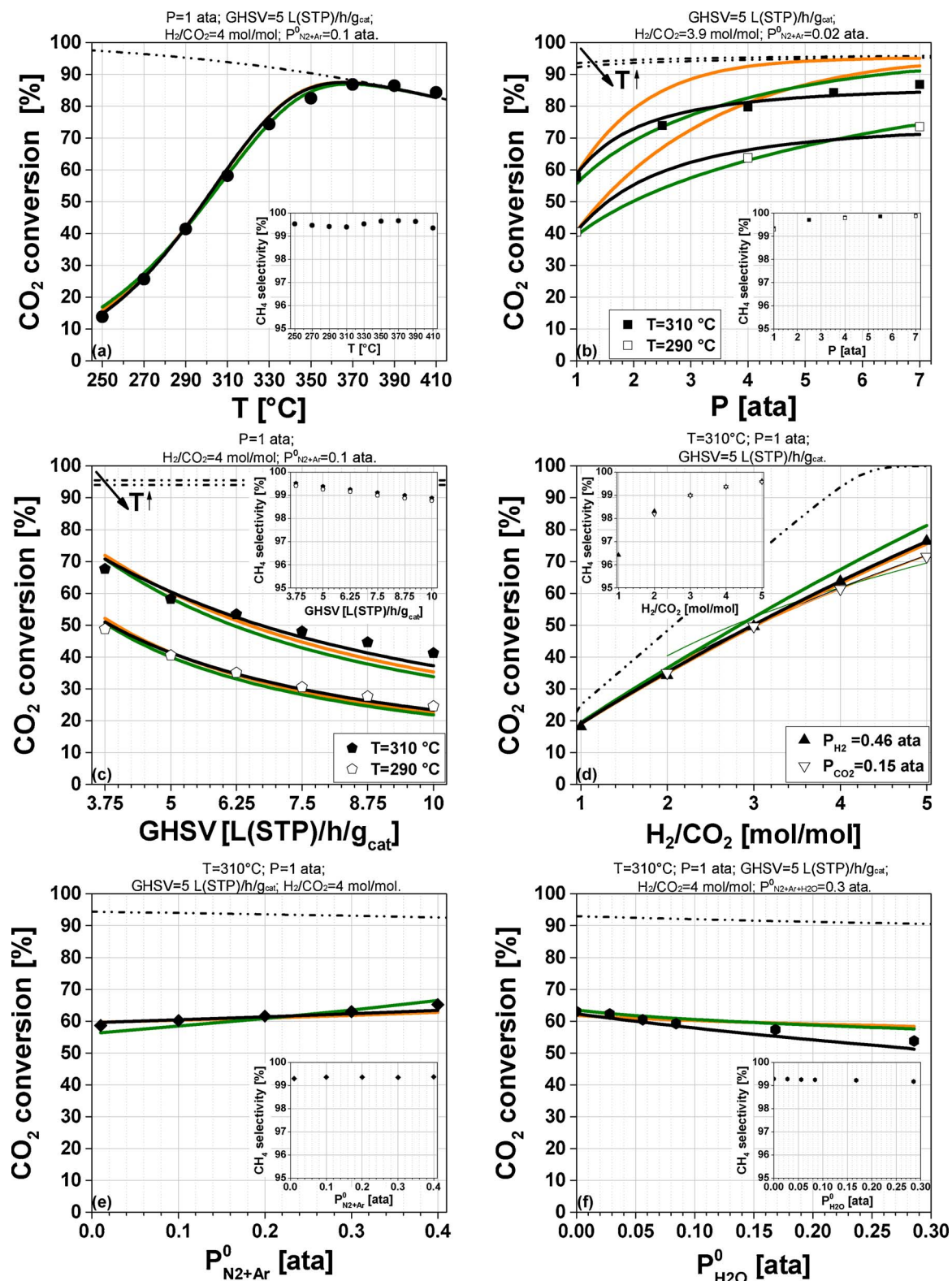


Fig. 5. Effect of (a) T, (b) P, (c) GHSV, (d) H_2/CO_2 , (e) $P^0_{\text{N}_2+\text{Ar}}$, (f) $P^0_{\text{H}_2\text{O}}$ on CO_2 conversion and (insets) CH_4 selectivity. Experimental CO_2 conversion data (symbols) are compared to model predictions (Lunde [Dataset 1] orange lines, Lunde [Dataset 2] green lines, LundeWI [Dataset 2] black lines). CO_2 conversion at thermodynamic equilibrium is also shown (dashed lines).

is shown in Fig. 5(c) at two different temperatures. By increasing GHSV from 3.75 to 10.00 L(STP)/h/g_{cat}, CO_2 conversion decreases from 68% to 41% at 310 °C, and from 49% to 25% at 290 °C. A decreasing trend by increasing GHSV is also observed in terms of CH_4 selectivity, but in

this case the effects are much less pronounced. Indeed, CH_4 selectivity decreases from 99.5% to 98.8% for both the investigated temperatures (inset Fig. 5(c)).

The decrease of CH_4 is compensated by CO , whose selectivity grows

up to 0.5% at the highest investigated GHSV. This result is in line with a reaction mechanism involving CO as reaction intermediate [29,35], and a CH₄ formation rate which is controlled by the slow conversion of CO₂ to CO. The very high selectivity to CH₄ measured in our experiments pointed out that, under the adopted process conditions, CO ad-species are very reactive and are rapidly hydrogenated. Accordingly, it is likely that lower Ru loadings [52] and/or higher space velocity [5] are required to increase the CO selectivity.

3.1.2.4. Effect of H₂/CO₂ inlet ratio and inert partial pressure.. The effects of H₂/CO₂ inlet ratio on CO₂ conversion and CH₄ selectivity, investigated either at constant P_{H₂}⁰ or at constant P_{CO₂}⁰, are shown in Fig. 5(d). By increasing the H₂/CO₂ inlet ratio from 1 to 5 at P_{H₂}⁰ = 0.46 ata, CO₂ conversion increases from 18% to 76%, while CH₄ selectivity which increases from 96.5% to 99.6%. Similar results have been observed keeping P_{CO₂}⁰ constant at 0.15 ata and varying P_{H₂}⁰. When increasing H₂/CO₂ from 2 to 5, CO₂ conversion increases from 35% to 72%, while CH₄ selectivity increases from 98.2% to 99.6%.

This behavior is in line with literature data showing that the H₂ feed content plays a fundamental role both on the adsorbed CO₂ and CO dissociation mechanisms and on the removal of OH ad-species from the catalyst surface [30,35].

The effect of the inert partial pressure is shown in Fig. 5(e). Interestingly, the inert fraction has a slight effect on CO₂ conversion. In addition, CH₄ selectivity remains pretty much constant while changing the amount of inert gas fed to the reactor (inset Fig. 5(e)).

3.1.2.5. Effect of water.. Fig. 6 shows the effect of water addition in the inlet feed on CO₂ conversion. The CO₂ conversion measured after 70 h on stream under dry conditions is stable at a value of 63%. When, at T.o.S. = 73 h, we started to co-feed water (P_{H₂O}⁰ = 0.08 ata, β = 0.47), CO₂ conversion shows a step decrease down to 59%. After this initial decrease, CO₂ conversion during the wet condition remains stable for the whole duration of the co-feeding (21 h). When water is removed from the feed (T.o.S. = 94 h), the initial activity is restored and CO₂ conversion goes back to its initial value. The same qualitative behavior is observed during all the co-feeding experiments, regardless the inlet flowrate of H₂O. On a quantitative base, Fig. 5(f) shows that for β value in the 0.16–1.58 range, CO₂ conversion decreases proportionally to the inlet water pressure.

Notably, CH₄ selectivity is not affected by water co-feeding, even

during experiments at high β values (inset Fig. 5(f)). These results are in line with those reported by Marwood et al. [30], who studied the effect of water on CO₂ methanation over a 2% Ru/TiO₂ catalyst using transient in-situ DRIFT experiments. They concluded that the presence of water decreases CO₂ conversion rate because H₂O inhibits the CO₂ activation rate, reducing the amount of CO adsorbed on Ru sites. Instead, no effects of H₂O were found on the consecutive stepwise hydrogenation of adsorbed CO to CH₄. Similar conclusions are also reported by Panagiotopoulou et al. [54], who showed that water addition has a strong effect on the CO₂ methanation kinetics, but does not influence CO methanation rate. Finally, an inhibition of water on the methanation kinetic is also described by some of the literature rate equations given in Table 1.

Our experimental data confirm that water addition inhibits CH₄ formation kinetics in CO₂ hydrogenation. Also, the observation that H₂O affects CO₂ conversion but not the process selectivity is in line with a kinetic effect of H₂O on the CO₂ activation (possibly going through adsorbed CO), but not on the CO ad-species desorption/hydrogenation.

3.2. Kinetic study

The values of kinetic parameters estimated by regression of the experimental data presented in Section 3.2.2 are listed in Table 4, along with the mean percentage error (MPE) on calculated CO₂ conversion. Fig. 7 shows the parity plots for all models investigated.

3.2.1. Lunde [Dataset 1]

Using the dataset 1 and the rate equation proposed in [22], an activation energy (E_A) of 68 kJ/mol was estimated along with n = 0.140 (Table 4). The E_A value is in good agreement with the typical values reported in the literature for Ru-based catalysts (Table 1). This is not the case of n, which was found to be lower than that reported by Lunde and Kester (0.225) [22,41], Ohya et al. (0.85) [42] and Brooks et al. (0.30) [43].

The parity plot shown in Fig. 7(a) points out that “Lunde [Dataset 1]” model well accounts for the effects of T (Fig. 5(a)), GHSV (Fig. 5(c)), H₂/CO₂ inlet ratio (Fig. 5(d)) and P_{N₂+Ar}⁰ (Fig. 5(e)) on CO₂ conversion. However, regardless the low MPE, the model tends to overestimate the kinetic effect of H₂O (Fig. 5(f)) and has serious difficulty to predict the effect of pressure (Fig. 5(b)). This suggests that the empirical rate expression “Lunde [Dataset 1]”, whose kinetic parameters are estimated

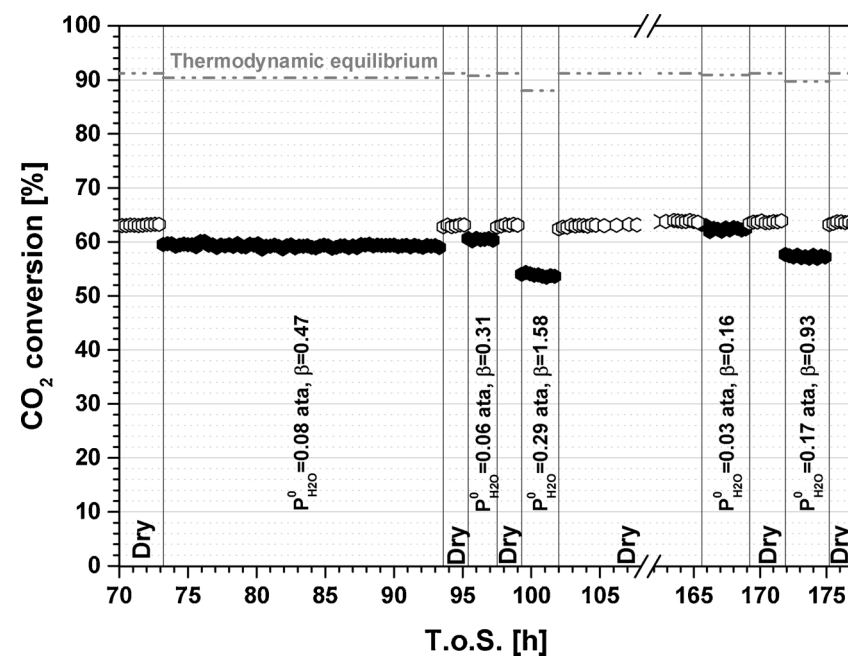
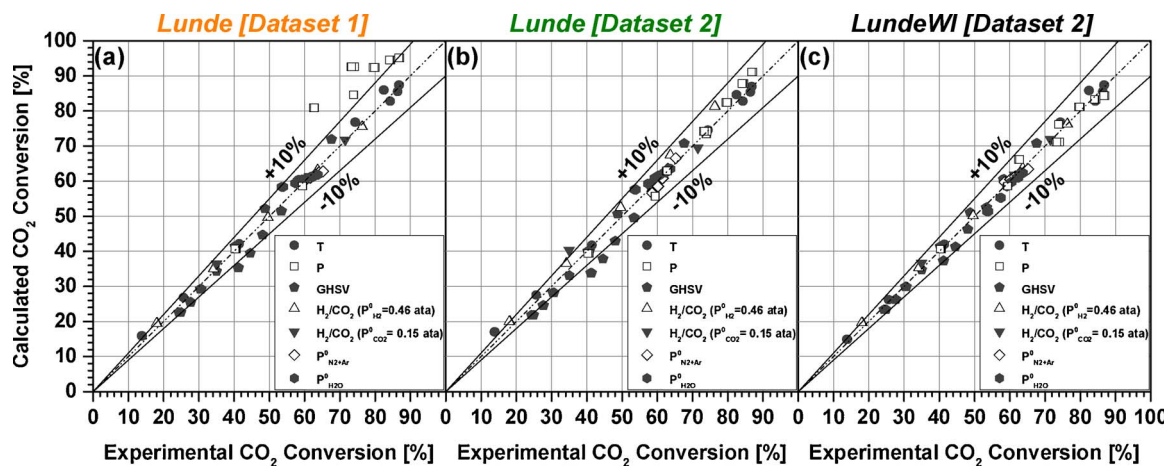


Fig. 6. CO₂ conversion as a function of T.o.S. with various water feed content.
(P_{H₂O}⁰ = 0–0.29 ata, T = 310 °C, P = 1 ata, GHSV = 5 L(STP)/h/g_{cat}, H₂/CO₂ = 4 mol_{H₂}/mol_{CO₂}, P_{N₂+Ar}⁰ + H₂O = 0.3 ata).

Fig. 7. Parity plots for calculated and experimental CO_2 conversion.

using data at atmospheric pressure, is not suited to describe data at high pressures. Such a conclusion may lead to reconsider some of the results reported in ref. [45,55–57] where performance of CO_2 methanation reactor was simulated for energetic and economic analyses of the PtG technology at pressures higher than atmospheric by using the model proposed by Lunde and Kester in [22].

3.2.2. Lunde [Dataset 2]

In order to overcome the limits of the approach described in Section 3.3.1, the same rate equation was fitted to all the data collected in this work, including those obtained at pressures over atmospheric (Dataset 2 in Table 2). The results of the regression are given in Table 4, labelled as “Lunde [Dataset 2]”. Not surprisingly, the estimated activation energy is 65 kJ/mol, a value close to that obtained in the previous regression. The n coefficient is instead 0.076, about half of the value of “Lunde [Dataset 1]”, one third of the value proposed Lunde and Kester [22,41] and more than 10 times lower than the value proposed by Ohya [42].

The parity plot (Fig. 7(b)) and the comparison of experimental and simulated process condition effects (Fig. 5) confirm that the rate equation proposed in [22], when fitted to the entire dataset, grants a much better fitting of experimental CO_2 conversion values. Focusing on the model description of P-effect (Fig. 5(b)), we note that after the new fitting, data at 290 °C are perfectly described by the model and data at 310 °C are described with an error lower than 5%.

Notably, the improvement in the description of high pressure data does not affect the ability of the model to describe temperature and water (Fig. 5(a) and (f), respectively) effect on CO_2 conversion and results only in a minor decrease of the quality of the fit of GHSV (Fig. 5(c)), $P_{\text{N}2+\text{Ar}}$ (Fig. 5(e)) and H_2/CO_2 ratio (Fig. 5(d)). Nevertheless this is a minor effect and, as a result, a decrease of the MPE (Table 4) is observed with respect to the previous fitting.

These results definitely prove that the kinetic expression proposed by Lunde and Kester [22] is very effective in predicting the CO_2 conversion at different process conditions, but indicate some limits of the kinetic parameters proposed so far in the literature [22,41–43], which may provide an inaccurate description of the catalyst performance during operations under pressure.

3.2.3. LundeWI [Dataset 2]

With the aim of further improving the kinetic description of CO_2 conversion rate during the methanation of concentrated CO_2 stream, a modified version of the model proposed by Lunde and Kester [22] is proposed in this work (Table 4), where an additional parameter (α) was added as denominator of the kinetic term representing the reduction of the active site number due to water adsorption.

The regression of this model against the complete input dataset (Dataset 2 in Table 2) brings to an estimated activation energy for the

Sabatier reaction equal to 75 kJ/mol, n and α values of 0.152 and 0.91 atm⁻¹, respectively (Table 4).

The parity plot shown in Fig. 7(c) shows the outstanding ability of this model in describing the experimental CO_2 conversion data, resulting in a MPE almost halved with respect to the models previously presented. Fig. 5 confirms that the effects of partial and total pressure on CO_2 conversion, as well as the temperature effect, are very well described in the entire range of process conditions investigated. Furthermore, the model correctly describes the effect of water and thus results in a better description of the space velocity effect on CO_2 conversion.

4. Conclusions

The performance of a commercial low loading (0.5 wt.%) Ru-based catalyst was investigated for the first time in a wide range of process conditions relevant to the *Power-to-Gas* application. The adopted catalyst was found to be stable, highly active and extremely selective to methane during CO_2 hydrogenation. By slightly increasing the pressure of the reactor, the thermodynamic equilibrium is shifted towards the products and the catalyst kinetics is boosted.

The presence of high amount of water does not deactivate the catalyst, but inhibits the Sabatier reaction kinetics. This makes in-situ strategies for water removal (such as sorption-enhanced process [58,59] or membrane reactors [42,60]) appealing and worth to be investigated.

The widely adopted kinetic expression proposed by Lunde and Kester in 1973 [22] is resulted adequate to describe the CO_2 conversion kinetics even at high pressure. A new set of kinetic parameters has to be used, however, to correctly describe the catalyst behavior from differential reactor conditions to high conversions limited by thermodynamic constraints.

A novel kinetic rate equation derived upon modification of the model proposed by [22] has been developed by explicitly accounting for a negative dependence on the partial pressure of water; the proposed rate equation further improves the model capability to simulate the catalyst performance in a wide range of process conditions relevant for *Power-to-Gas* technology.

References

- [1] M. Aresta, A. Dibenedetto, A. Angelini, Catalysis for the valorization of exhaust carbon: from CO_2 to chemicals, materials, and fuels. technological use of CO_2 , Chem. Rev. 114 (2014) 1709–1742, <http://dx.doi.org/10.1021/cr4002758>.
- [2] E.A. Quadrelli, G. Centi, J.L. Duplan, S. Perathoner, Carbon dioxide recycling: emerging large-scale technologies with industrial potential, ChemSusChem 4 (2011) 1194–1215, <http://dx.doi.org/10.1002/cssc.201100473>.
- [3] M. Götz, J. Lefebvre, F. Mörs, A. McDaniel Koch, F. Graf, S. Bajohr, et al.,

Renewable Power-to-Gas: a technological and economic review, *Renew. Energy* 85 (2016) 1371–1390, <http://dx.doi.org/10.1016/j.renene.2015.07.066>.

- [4] J. Gao, Q. Liu, F. Gu, B. Liu, Z. Zhong, F. Su, Recent advances in methanation catalysts for the production of synthetic natural gas, *RSC Adv.* 5 (2015) 22759–22776, <http://dx.doi.org/10.1039/C4RA16114A>.
- [5] C. Janke, M.S. Duyar, M. Hoskins, R.J. Farrauto, Catalytic and adsorption studies for the hydrogenation of CO₂ to methane, *Appl. Catal. B Environ.* 152–153 (2014) 184–191, <http://dx.doi.org/10.1016/j.apcatb.2014.01.016>.
- [6] S. Rieke, Erste Industrielle Power-to-Gas-Anlage Mit 6 Megawatt, (2013).
- [7] K. Osman, T. Götz, A. Schönrock, Das e-gas-Projekt Am Biogasanlagen Standort in Werlte, (2014).
- [8] J. Specht, V. Breloch, B. Frick, U. Sturmer, Technical realization of Power-to-Gas technology (P2G): production of substitute natural gas by catalytic methanation of H₂/CO₂, in: R. Van Baschusen (Ed.), *Nat. Gas Renew. Methane Powertrains – Futur. Strateg. a. Clim. Mobil.* Springer, 2016, pp. 141–167, <http://dx.doi.org/10.1007/978-3-319-23225-6>.
- [9] S. Rönsch, J. Schneider, S. Matthischke, M. Schlüter, M. Götz, J. Lefebvre, et al., Review on methanation – From fundamentals to current projects, *Fuel* 166 (2016) 276–296, <http://dx.doi.org/10.1016/j.fuel.2015.10.111>.
- [10] S. Sahebdelfar, M. Takht Ravanchi, Carbon dioxide utilization for methane production: a thermodynamic analysis, *J. Pet. Sci. Eng.* 134 (2015) 14–22, <http://dx.doi.org/10.1016/j.petrol.2015.07.015>.
- [11] W. Wang, J. Gong, Methanation of carbon dioxide: an overview, *Front. Chem. Eng. China* 5 (2011) 2–10, <http://dx.doi.org/10.1007/s11705-010-0528-3>.
- [12] G.A. Mills, F.W. Steffgen, Catalytic methanation, *Catal. Rev. Sci. Eng.* 8 (1974) 159–210, <http://dx.doi.org/10.1080/01614947408071860>.
- [13] C.G. Visconti, M. Martinelli, L. Falbo, L. Fratalocchi, L. Lietti, CO₂ hydrogenation to hydrocarbons over Co and Fe-based Fischer-Tropsch catalysts, *Catal. Today* 277 (2016) 161–170, <http://dx.doi.org/10.1016/j.cattod.2016.04.010>.
- [14] L. Seguin, *Methanation of Synthesis Gas (Advances in Chemistry Series, 146)*, (1975).
- [15] J. Liu, C. Li, F. Wang, S. He, H. Chen, Y. Zhao, et al., Enhanced low-temperature activity of CO₂ methanation over highly-dispersed Ni/TiO₂ catalyst, *Catal. Sci. Technol.* 3 (2013) 2627, <http://dx.doi.org/10.1039/c3cy00355h>.
- [16] M. Agnelli, M. Kolb, C. Nicot, C. Mirodatos, Sintering of a Ni-based catalyst during CO hydrogenation kinetics and modeling, in: C.H. Bartholomew, J.B. Butt (Eds.), *Catal. Deactiv.* Elsevier, B.V, Amsterdam, 1991, pp. 605–612.
- [17] I. Fechete, J.C. Vedrine, Nanoporous materials as new engineered catalysts for the synthesis of green fuels, *Molecules* 20 (2015) 5638–5666, <http://dx.doi.org/10.3390/molecules20045638>.
- [18] W. Wang, S. Wang, X. Ma, J. Gong, Recent advances in catalytic hydrogenation of carbon dioxide, *Chem. Soc. Rev.* 40 (2011) 3703–3727, <http://dx.doi.org/10.1039/c1cs15008a>.
- [19] M.A.A. Aziz, A.A. Jalil, S. Triwahyono, A. Ahmad, CO₂ methanation over heterogeneous catalysts: recent progress and future prospects, *Green Chem.* 17 (2015) 2647–2663, <http://dx.doi.org/10.1039/C5GC00119F>.
- [20] F. Koschany, D. Schlereth, O. Hinrichsen, On the kinetics of the methanation of carbon dioxide on coprecipitated NiAl(O)_x, *Appl. Catal. B Environ.* 181 (2016) 504–516, <http://dx.doi.org/10.1016/j.apcatb.2015.07.026>.
- [21] G. Garbarino, D. Belotti, P. Riani, L. Magistri, G. Busca, Methanation of carbon dioxide on Ru/Al₂O₃ and Ni/Al₂O₃ catalysts at atmospheric pressure: catalysts activation, behaviour and stability, *Int. J. Hydrogen Energy* 40 (2015) 9171–9182, <http://dx.doi.org/10.1016/j.ijhydene.2014.05.111>.
- [22] P.J. Lunde, F.L. Kester, Rates of methane formation from carbon dioxide and hydrogen over a ruthenium catalyst, *J. Catal.* 30 (1973) 423–429, [http://dx.doi.org/10.1016/0021-9517\(73\)90159-0](http://dx.doi.org/10.1016/0021-9517(73)90159-0).
- [23] F. Solymosi, A. Erdőhelyi, Hydrogenation of CO₂ to CH₄ over alumina-supported noble metals, *J. Mol. Catal.* 8 (1980) 471–474, [http://dx.doi.org/10.1016/0304-5102\(80\)80086-1](http://dx.doi.org/10.1016/0304-5102(80)80086-1).
- [24] C. de Leitenburg, A. Trovarelli, J. Kaspar, A temperature-programmed and transient kinetic study of CO₂ activation and methanation over CeO₂ supported noble metals, *J. Catal.* 166 (1997) 98–107, <http://dx.doi.org/10.1006/jcat.1997.1498>.
- [25] P. Panagiotopoulou, D.I. Kondarides, X.E. Verykios, Selective methanation of CO over supported noble metal catalysts: effects of the nature of the metallic phase on catalytic performance, *Appl. Catal. A Gen.* 344 (2008) 45–54, <http://dx.doi.org/10.1016/j.apcata.2008.03.039>.
- [26] V. Barbarossa, C. Bassano, P. Deiana, G. Vanga, CO₂ conversion to CH₄, in: G. de Falco (Ed.), *CO₂ A Valuable Source Carbon*, Springer-Verlag, 2013, pp. 123–145, , <http://dx.doi.org/10.1007/978-1-4471-5119-7>.
- [27] F.S. Karn, J.F. Shultz, R.B. Anderson, Hydrogenation of carbon monoxide and carbon dioxide on supported ruthenium catalysts at moderate pressures, *Ind. Eng. Chem. Prod. Res. Dev.* 4 (1965) 265–269, <http://dx.doi.org/10.1021/1360016a014>.
- [28] J.G. Highfield, P. Ruterana, K.R. Thampi, M. Graetzel, Catalyst characterization and IN SITU studies of carbon dioxide methanation over ruthenium supported on titania, in: C. Morterra, A.Z. And, G. Costa (Eds.), *Struct. React. Surfaces*, 1989, p. 469.
- [29] M.R. Prairie, A. Renken, J.G. Highfield, K. Ravindranathan Thampi, M. Grätzel, A fourier transform infrared spectroscopic study of CO₂ methanation on supported ruthenium, *J. Catal.* 129 (1991) 130–144, [http://dx.doi.org/10.1016/0021-9517\(91\)90017-X](http://dx.doi.org/10.1016/0021-9517(91)90017-X).
- [30] M. Marwood, R. Doepper, M. Prairie, A. Renken, Transient drift spectroscopy for the determination of the surface-reaction kinetics of CO₂ methanation, *Chem. Eng. Sci.* 49 (1994) 4801–4809, [http://dx.doi.org/10.1016/S0009-2509\(05\)80060-0](http://dx.doi.org/10.1016/S0009-2509(05)80060-0).
- [31] S. Eckle, H.G. Anfang, R.J. Behm, Reaction intermediates and side products in the methanation of CO and CO₂ over supported Ru catalysts in H₂-Rich reformate gases, *J. Phys. Chem. C* 115 (2011) 1361–1367, <http://dx.doi.org/10.1021/jp108106t>.
- [32] M.A. Henderson, S.D. Worely, An infrared study of the hydrogenation of carbon dioxide on supported rhodium catalysts, *J. Phys. Chem.* 89 (1985) 1417–1423, <http://dx.doi.org/10.1021/j100254a023>.
- [33] E. Zagli, J.L. Falconer, Carbon dioxide adsorption and methanation on ruthenium, *J. Catal.* 69 (1981) 1–8, [http://dx.doi.org/10.1016/0021-9517\(81\)90122-6](http://dx.doi.org/10.1016/0021-9517(81)90122-6).
- [34] M. Marwood, R. Doepper, A. Renken, In-situ surface and gas phase analysis for kinetic studies under transient conditions The catalytic hydrogenation of CO₂, *Appl. Catal. A Gen.* 151 (1997) 223–246, [http://dx.doi.org/10.1016/S0926-860X\(96\)00267-0](http://dx.doi.org/10.1016/S0926-860X(96)00267-0).
- [35] X. Wang, Y. Hong, H. Shi, J. Szanyi, Kinetic modeling and transient DRIFTS-MS studies of CO₂ methanation over Ru/Al₂O₃ catalysts, *J. Catal.* 343 (2016) 185–195, <http://dx.doi.org/10.1016/j.jcat.2016.02.001>.
- [36] F. Solymosi, A. Erdőhelyi, M. Kocsis, Methanation of CO₂ on supported Ru catalysts, *J. Chem. Soc. Faraday Trans.* 77 (1981) 1003–1012.
- [37] Y. Traa, J. Weitkamp, Kinetics of the methanation of carbon dioxide over ruthenium on titania, *Chem. Eng. Technol.* 21 (1999) 291–293.
- [38] M. Kuśmierz, Kinetic study on carbon dioxide hydrogenation over Ru/γ-Al₂O₃ catalysts, *Catal. Today* 137 (2008) 429–432, <http://dx.doi.org/10.1016/j.cattod.2008.03.003>.
- [39] K. Takeishi, K. Aika, Comparison of carbon dioxide and carbon monoxide with respect to hydrogenation on Raney ruthenium catalysts, *Appl. Catal. A Gen.* 133 (1995) 31–45, [http://dx.doi.org/10.1016/0926-860X\(95\)00143-3](http://dx.doi.org/10.1016/0926-860X(95)00143-3).
- [40] M.S. Duyar, A. Ramachandran, C. Wang, R.J. Farrauto, Kinetics of CO₂ methanation over Ru/Al₂O₃ and implications for renewable energy storage applications, *J. CO₂ Util.* 12 (2015) 27–33, <http://dx.doi.org/10.1016/j.jcou.2015.10.003>.
- [41] P.J. Lunde, F.L. Kester, Carbon dioxide methanation on a ruthenium catalyst, *Ind. Eng. Chem. Process Des. Dev.* 13 (1974) 27–33, <http://dx.doi.org/10.1021/i260049a005>.
- [42] H. Ohya, J. Fun, H. Kawamura, K. Itoh, H. Ohashi, M. Aihara, et al., Methanation of carbon dioxide by using membrane reactor integrated with water vapor permeable membrane and its analysis, *J. Membr. Sci.* 131 (1997) 237–247, [http://dx.doi.org/10.1016/S0376-7388\(97\)00055-0](http://dx.doi.org/10.1016/S0376-7388(97)00055-0).
- [43] K.P. Brooks, J. Hu, H. Zhu, R.J. Kee, Methanation of carbon dioxide by hydrogen reduction using the Sabatier process in microchannel reactors, *Chem. Eng. Sci.* 62 (2007) 1161–1170, <http://dx.doi.org/10.1016/j.ces.2006.11.020>.
- [44] I. Kalaitzidou, M. Makri, D. Theleritis, A. Katsaounis, C.G. Vayenas, Comparative study of the electrochemical promotion of CO₂ hydrogenation on Ru using Na⁺, K⁺, H⁺ and O²⁻ conducting solid electrolytes, *Surf. Sci.* 646 (2016) 194–203, <http://dx.doi.org/10.1016/j.susc.2015.09.011>.
- [45] L. Kiewitz, J. Thöming, Predicting optimal temperature profiles in single-stage fixed-bed reactors for CO₂-methanation, *Chem. Eng. Sci.* 132 (2015) 59–71, <http://dx.doi.org/10.1016/j.ces.2015.03.068>.
- [46] M. Schoder, U. Armbruster, A. Martin, Heterogen katalysierte Hydrierung von Kohlenstoffdioxid zu Methan unter erhöhten drucken, *Chemie Ingenieur Technik* 85 (2013) 344–352, <http://dx.doi.org/10.1002/cite.201200112>.
- [47] D.E. Mears, Tests for transport limitations in experimental catalytic reactors, *Ind. Eng. Chem. Process Des. Dev.* 10 (1971) 541–547, <http://dx.doi.org/10.1021/i260040a020>.
- [48] N. Wakao, S. Kagei, *Heat and Mass Transfer in Packed Beds*, Gordon and Breach Science Publishers, 1982.
- [49] G.B. Ferraris, G. Donati, A powerful method for Hougen-Watson model parameter estimation with integral conversion data, *Chem. Eng. Sci.* 29 (1974) 1504–1509, [http://dx.doi.org/10.1016/0009-2509\(74\)80177-6](http://dx.doi.org/10.1016/0009-2509(74)80177-6).
- [50] A.C. Hindmarsh, *ODEPACK, Systematized Collection of ODE Solvers*, Scientific Computing Amsterdam, NorthHolland, 1983, pp. 55–64.
- [51] V. Mazzieri, F. Coloma-Pascual, A. Arcoya, P.C. L'Argentiére, N.S. Fígoli, XPS, FTIR and TPR characterization of Ru/Al₂O₃ catalysts, *Appl. Surf. Sci.* 210 (2003) 222–230, [http://dx.doi.org/10.1016/S0169-4332\(03\)00146-6](http://dx.doi.org/10.1016/S0169-4332(03)00146-6).
- [52] J.H. Kwak, L. Kovárik, J. Szanyi, CO₂ reduction on supported Ru/Al₂O₃ catalysts: cluster size dependence of product selectivity, *ACS Catal.* 3 (2013) 2449–2455, <http://dx.doi.org/10.1021/cs400381f>.
- [53] R.B. Anderson, *The Fischer Tropsch Synthesis*, Academic Press Orlando, 1984.
- [54] P. Panagiotopoulou, D.I. Kondarides, X.E. Verykios, Selective methanation of CO over supported Ru catalysts, *Appl. Catal. B Environ.* 88 (2009) 470–478, <http://dx.doi.org/10.1016/j.apcatb.2008.10.012>.
- [55] F. Gutiérrez-Martín, L.M. Rodríguez-Antón, Power-to-SNG technology for energy storage at large scales, *Int. J. Hydrogen Energy* 41 (2016) 19290–19303, <http://dx.doi.org/10.1016/j.ijhydene.2016.07.097>.
- [56] O.S. Buchholz, A.G.J. Van Der Ham, R. Veneman, D.W.F. Brilman, S.R.A. Kersten, Power-to-Gas Storing surplus electrical energy. A design study, *Energy Procedia* 63 (2014) 7993–8009, <http://dx.doi.org/10.1016/j.egypro.2014.11.836>.
- [57] M. De Saint Jean, P. Baurens, C. Bouallou, Parametric study of an efficient renewable power-to-substitute-natural-gas process including high-temperature steam electrolysis, *Int. J. Hydrogen Energy* 39 (2014) 17024–17039, <http://dx.doi.org/10.1016/j.ijhydene.2015.03.066>.
- [58] S. Walpurger, G.D. Elzinga, J.W. Dijkstra, M. Sarić, W.G. Haije, Sorption enhanced methanation for substitute natural gas production: experimental results and thermodynamic considerations, *Chem. Eng. J.* 242 (2014) 379–386, <http://dx.doi.org/10.1016/j.cej.2013.12.045>.
- [59] A. Borgschulte, N. Gallandat, B. Probst, R. Suter, E. Callini, D. Ferri, et al., Sorption enhanced CO₂ methanation, *Phys. Chem. Chem. Phys.* 15 (2013) 9620–9625, <http://dx.doi.org/10.1039/c3cp51408k>.
- [60] D. Schlereth, O. Hinrichsen, A fixed-bed reactor modeling study on the methanation of CO₂, *Chem. Eng. Res. Des.* 92 (2014) 702–712, <http://dx.doi.org/10.1016/j.cherd.2013.11.014>.